Characterization of High Phosphate Radioactive Tank Waste and Simulant Development

ARTICLE *in* ENVIRONMENTAL SCIENCE AND TECHNOLOGY · OCTOBER 2009

Impact Factor: 5.33 · DOI: 10.1021/es9013745 · Source: PubMed

5 AUTHORS, INCLUDING:

Edgar C. Buck
Pacific Northwest National Laboratory
188 PUBLICATIONS **1,520** CITATIONS

Characterization of High Phosphate Radioactive Tank Waste and Simulant Development

GREGG J. LUMETTA,*
BRUCE K. MCNAMARA, EDGAR C. BUCK,
SANDRA K. FISKUM, AND
LANÉE A. SNOW

Pacific Northwest National Laboratory, P.O. Box 999, MSIN P7-25, Richland, Washington 99352

Received May 15, 2009. Revised manuscript received August 24, 2009. Accepted August 26, 2009.

A sample of high-level radioactive tank waste was characterized to provide a basis for developing a waste simulant. The simulant is required for pilot-scale testing of pretreatment processes in a nonradiological facility. The waste material examined was derived from the bismuth phosphate process, which was the first industrial process implemented to separate plutonium from irradiated nuclear fuel. The bismuth phosphate process sludge is a complex mixture rich in bismuth, iron, sodium, phosphorus, silicon, and uranium. The form of phosphorus in this particular tank waste material is of specific importance because that is the primary component (other than water-soluble sodium salts) that must be removed from the high-level waste solids by pretreatment. This work shows unequivocally that the phosphorus in this waste material is not present as bismuth phosphate. Rather, the phosphorus appears to be incorporated mostly into an amorphous iron(III) phosphate phase. The bismuth in the sludge solids is best described as $BiFeO_3$. The behavior of phosphorus during caustic leaching of the bismuth phosphate process sludge solids is also discussed.

Introduction

During World War II and the Cold War, a very large amount of highly radioactive waste was generated during the production of plutonium for weapons. These wastes are distributed across numerous sites worldwide. Although much of the radioactive material generated during these operations was stored in tanks, some of the radioactive material was released directly to the environment. Furthermore, most of the storage tanks containing the bulk of the radioactive material have exceeded their design lifetime, and many of the tanks have already leaked part of their contents to the environment. Thus, there is great impetus to retrieve the radioactive tank wastes and process them into stable waste forms suitable for disposal.

In the United States, most of the legacy waste from past plutonium production is located at the Savannah River Site in South Carolina and at the Hanford Site in Washington State. Indeed, restoration of the U.S. Department of Energy's (DOE's) Hanford Site is one of the largest environmental remediation projects ever undertaken (*1*). Disposal of the ~200,000 m^3 of radioactive tank waste is the most daunting challenge facing Hanford (*2*). Sixty-seven of the 177 underground storage tanks at Hanford have leaked, and there is mounting concern about the mobility of the radionuclides released to the environment during these leaks and potential future leaks. For these reasons, DOE has commissioned the design and construction of the Hanford Tank Waste Treatment and Immobilization Plant (WTP).

For a schematic illustration of the primary functions to be performed in the WTP, see Figure S1 in the Supporting Information. Initially, the low-activity waste (LAW) liquid stream will be removed from the high-level waste (HLW) solids by ultrafiltration. The concentrated HLW solids will be pretreated by leaching with caustic (aqueous NaOH), and in some cases by oxidative leaching (with permanganate), to dissolve and remove components that would otherwise limit HLW loading in the immobilized waste glass. The function of caustic leaching is to convert the aluminum, phosphorus, and sulfur in the HLW solids into soluble forms, thereby removing these components from the HLW vitrification feed (*3*). The function of oxidative leaching is to oxidize the chromium from the insoluble Cr(III) form to highly soluble Cr(VI), which can be routed to the LAW stream (*4, 5*). Following pretreatment, the HLW solids will be vitrified into a borosilicate glass matrix. The LAW stream will also be immobilized as borosilicate glass after the ^{137}Cs has been removed by ion exchange (*6*). The vitrified HLW will be disposed of in a national geologic repository while the immobilized LAW will be disposed of by burial at the Hanford Site.

The development and testing of the processes to be implemented in the Hanford WTP are complicated by the high radioactivity associated with the waste materials. Indeed, the radioactivity precludes pilot-scale testing with actual tank waste. To gain confidence in the processes to be installed in the WTP, testing will be performed in a nonradioactive pilot-scale facility with simulated waste material, and small laboratory verification tests will be conducted with actual radioactive tank waste. For this approach to succeed, tank-waste simulants must be developed that accurately mimic the behavior of the actual wastes. Depending on the specific purpose of the simulants, the simulants must mimic the chemical properties and/or the physical properties of the actual tank waste. Developing such simulants is challenging because the HLW solids in the Hanford tank wastes are complex mixtures of inorganic salts and minerals (*7*). Furthermore, the composition of the HLW solids is highly variable because of the different production processes that were deployed at Hanford.

In this paper, we describe a case study in developing a simulant for a highly hazardous material to support environmental remediation efforts. Specifically, we report the characterization of one type of Hanford tank waste—the Bismuth Phosphate Process (BPP) sludge. This waste was produced during operation of the bismuth phosphate process, which was the very first plutonium processing method ever used at an industrial scale (*8*). This process produced very large quantities of waste material because it involved repeated precipitation cycles to recover the plutonium from irradiated fuel in pure form. The byproduct from this process was neutralized with sodium hydroxide and stored in carbon-steel tanks. The precipitated solid that formed in these waste tanks is the subject of this paper.

The objective of the work described here is to characterize the BPP sludge to guide development of a waste simulant suitable for testing in a nonradioactive pilot plant. Small samples of the BPP sludge were characterized by a combination of chemical and radiochemical methods along with Fourier-transform infrared (FTIR) spectroscopy,

* Corresponding author e-mail: gregg.lumetta@pnl.gov.

10.1021/es9013745 CCC: $40.75
Published on Web 09/11/2009

scanning electron microscopy (SEM), transmission electron microscopy (TEM), optical microscopy, thermogravimetric analysis (TGA), and differential thermal analysis (DTA). Analogous measurements were made for potential waste simulant materials. The properties of the actual tank waste material are compared to those for the candidate simulant materials.

Experimental Section

Materials and Methods. Bismuth phosphate and $FePO_4 \cdot xH_2O$ were obtained from Alfa Aesar (Ward Hill, MA). Bismuth oxyhydroxide, bismuth oxide, and $BiFeO_3$ were prepared and characterized as described in the literature (*9, 10*).

A detailed description of the preparation of the composite sample of BPP sludge was previously published (*11*). Sample materials from three different tanks were used to make the composite, but the bulk of the material (93%) came from Hanford Tank 241-B-104, with minor contributions from Tanks 241-BX-112 (4%) and 241-T-104 (3%). A total of 1889 g of tank waste sample material was mixed with 968 g of deionized water to yield 2857 g of slurry. This slurry was homogenized with a mechanical stirrer and divided into several aliquots for various testing and characterization activities.

A portion of the BPP sludge sample was washed repeatedly with 0.01 M NaOH to remove the water-soluble components from the HLW solids. The washed solids were fused, then dissolved to support chemical and radiochemical analysis. For the fusion method, 0.1−0.2 g dry solids was combined with the flux mixture (KOH/KNO_3) and fused at 550 °C for 1 h in a nickel crucible. The fused material was acidified with HNO_3, diluted to 100 mL with deionized water, and then split for elemental and radionuclide analyses.

Elemental analysis was performed by inductively coupled argon plasma optical emission spectrometry (ICP-OES). Uranium was determined by kinetic phosphorescence analysis (KPA). Gamma-emitting radionuclides were determined by standard gamma spectroscopy techniques using a high-purity germanium detector. Plutonium isotopes were determined by alpha spectroscopy on sample mounts produced by coprecipitation of PuF_3 with LaF_3 after radiochemical separation of the plutonium. Strontium-90 was determined by liquid scintillation counting after this isotope was separated from the analyte matrix.

The water-insoluble BPP sludge solids were prepared for TGA/DTA analysis by adding a portion of the dried solids directly to quartz pans. The TGA/DTA analyses were performed on a Seiko model 5200. All scans of the tank waste material were run at 5 °C/min to 900 °C in dry air. The cooling curve was run at 5 °C/min to correct for buoyancy in the TGA and DTA baselines on heating.

FTIR spectra were recorded on a Bruker Alpha-P spectrometer equipped with a diamond attenuated total reflectance (ATR) cell. The samples were ground to a powder with a spatula. The powder was suspended in acetone, and the suspension was placed on the ATR crystal. Spectral acquisition was performed after the acetone evaporated.

SEM was performed using an Amray model 1610T SEM. For the SEM examination, the sample was placed on a carbon tape supported by an aluminum pedestal mount. In selected cases, the mount was carbon-coated to reduce charging. Selected sample areas were evaluated by energy dispersive X-ray spectroscopy (EDS) for qualitative elemental composition. Samples to be examined by TEM were prepared by dispersing in methanol, extracting a drop of this slurry into a second vial containing methanol, and depositing a drop of this second solution onto a lacy carbon TEM grid. The images and electron diffraction patterns were obtained with the FEI Tecnai 30S-Twin. Elemental compositions were also obtained from the TEM images using EDS.

TABLE 1. Chemical and Radiochemical Composition of the Dried Water-Insoluble BPP Sludge Solids

analyte	conc., wt%[a]	analyte	conc., μCi/g
Al	2.6	^{137}Cs	3.0×10^{01}
Bi	12.1	^{60}Co	1.2×10^{-03}
Cr	0.5	^{241}Am	6.8×10^{-02}
Fe	10.9	^{238}Pu	6.8×10^{-03}
Na	13.4	$^{239+240}$Pu	6.9×10^{-01}
P	10.1	^{90}Sr	4.5×10^{01}
S[b]	0.2		
Si	6.0		
U	1.0		

[a] Only those components found in excess of 0.1 wt % are reported. [b] The sulfur concentration was near the instrument detection limit, so the uncertainty in this value is >15%.

Preparation of Hydrous Iron(III) Phosphate. $Na_3PO_4 \cdot 12H_2O$ (0.5187 g, 1.364 mmol; Aldrich) was dissolved in 3 mL of deionized water. $Fe(NO_3)_3 \cdot 9H_2O$ (0.4909 g, 1.125 mmol; Fisher) was dissolved in 0.6 mL of deionized water. The ferric nitrate solution was filtered through a 0.2-μm nylon syringe filter with the filtrate dropping into the stirring solution of sodium phosphate. The beige precipitate was separated from the solution phase by centrifuging and decanting, then was washed repeatedly with 3−4-mL portions of deionized water and dried at 45 °C. Because the exact nature of this material is not known, we refer to it as "hydrous iron(III) phosphate" throughout this paper.

Caustic Leaching of Bismuth Phosphate Process Sludge Solids. The specific leaching conditions used are given in Table S1. Aliquots of the washed solids were divided among eight 125-mL high-density polyethylene (HDPE) bottles with each aliquot containing ~0.95 g of water-insoluble solids. Sodium hydroxide (19 M; 5.3 mL to yield 1 M NaOH and 15.8 mL to yield 3 M NaOH) was added to each leaching sample along with enough deionized water to give a total volume of 100 mL. The leaching temperature (40, 60, or 80 °C) was maintained with temperature-controlled aluminum block heating. The heating block was supported on a J-KEM BTS-3500 digital benchtop shaker, which provided agitation of the mixtures. The liquid phase was sampled, cooled, and filtered for ICP-OES analysis at designated time intervals to monitor the leaching behavior of the different waste components.

Results and Discussion

Chemical and Radiochemical Composition of the Bismuth Phosphate Process Sludge Solids. Table 1 summarizes the chemical and radiochemical composition of the washed and dried BPP sludge solids. The solids are dominated by the presence of Bi, Fe, Na, P, and Si. The gamma activity of the BPP sludge solids is nearly all attributable to ^{137}Cs ($t_{1/2}$ = 30.2 y), or more accurately to its daughter product ^{137m}Ba ($t_{1/2}$ = 2.6 min; γ energy = 662 keV). The beta activity is due to ^{137}Cs plus ^{90}Sr ($t_{1/2}$ = 28.6 y) and its daughter ^{90}Y ($t_{1/2}$ = 64.1 h). The alpha activity is mainly attributed to ^{241}Am ($t_{1/2}$ = 432 y) and ^{239}Pu ($t_{1/2}$ = 24,100 y) and/or ^{240}Pu ($t_{1/2}$ = 6570 y). The isotopes ^{239}Pu and ^{240}Pu cannot be resolved by alpha spectroscopy, and the ratio of these two Pu isotopes is unknown.

FTIR Spectroscopic Characterization. Phosphorus is the component of most interest with regard to developing a simulant for the BPP sludge solids. Because of the relatively low tolerance for P in the HLW vitrification feed at the WTP, the caustic-leaching process must remove most of the P from the solids. Knowledge of the chemical form of phosphorus in the BPP sludge solids was needed to guide simulant

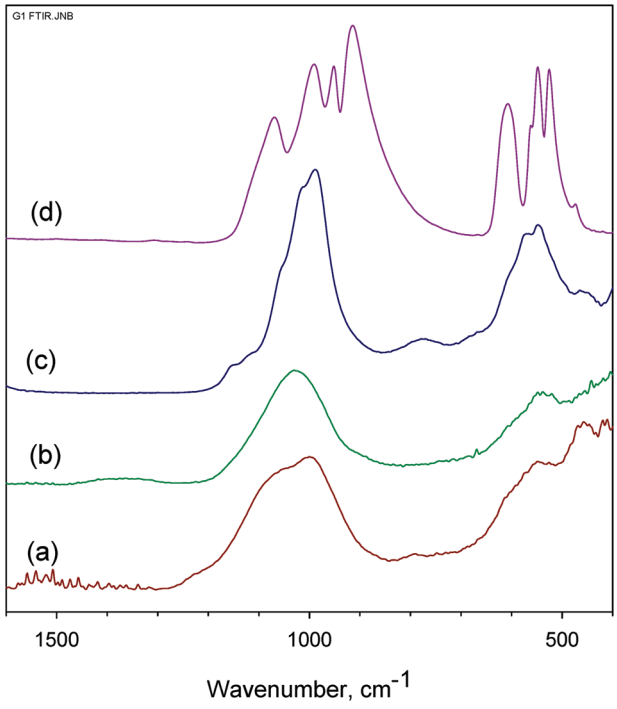

FIGURE 1. FTIR spectra of (a) the washed BPP sludge solids, (b) hydrous iron(III) phosphate prepared by mixing $Fe(NO_3)_3$ solution with Na_3PO_4 solution, (c) commercially procured $FePO_4 \cdot xH_2O$, and (d) $BiPO_4$.

development. The BPP sludge solids were examined by FTIR spectroscopy to gain an understanding of the chemical form of P in the waste. Figure 1 presents the FTIR spectrum of the washed BPP sludge solids along with the spectra for some candidate phosphorus-containing compounds. The compounds shown for comparison are commercially procured $FePO_4 \cdot xH_2O$ and $BiPO_4$, and the hydrous iron(III) phosphate.

The FTIR spectrum of the BPP sludge solids is consistent with an iron(III) phosphate species. Although there is not a perfect match with the hydrous iron(III) phosphate, this material seems to best match the FTIR spectrum of the waste material based on the broad P−O stretching bands in the region 850−1200 cm^{-1}. The crystalline $FePO_4 \cdot xH_2O$ displays more narrow P−O stretching bands than the tank waste solids, so this form of iron(III) phosphate is not dominant in the actual waste. Differences between the FTIR spectrum of the tank waste solids and that of the hydrous iron(III) phosphate are not surprising since the product formed by reacting ferric ion with aqueous sodium phosphate can only approximately be considered to be $FePO_4 \cdot xH_2O$ (amorphous), and its composition depends upon the pH of the solution during precipitation (*12*). The hydrous iron(III) phosphate product prepared in this work was undoubtedly formed under conditions that were different from that for the actual tank waste, so slight differences in their FTIR spectra should be expected. Furthermore, the actual tank waste sample contains other components, including compounds of silicon, which would be expected to display Si−O stretching bands in the same region of the FTIR spectrum (*13, 14*). Overlapping of these bands complicates the spectral interpretation. The FTIR spectra do not support the presence of $BiPO_4$ in the BPP sludge since the FTIR spectrum of $BiPO_4$ is clearly much different than that of the actual sludge solids. The FTIR spectrum of the BPP sludge solids does not provide insight into the nature of the bismuth phases present in the material. Possible candidates include Bi_2O_3 and $Bi(OH)_3$. The FTIR spectrum of Bi_2O_3 is essentially featureless above 600 cm^{-1}. The FTIR spectrum of $Bi(OH)_3$, prepared by mixing bismuth nitrate with concentrated ammonium hydroxide, indicated broad bands at ~1340 and 885 cm^{-1}. These bands might be attributable to residual nitrate in the precipitated $Bi(OH)_3$, but regardless, neither band is evident in the spectrum of the BPP sludge.

SEM and TEM Examination. The BPP sludge solids were mostly amorphous to X-rays, so definitive identification of chemical phases present could not be achieved by X-ray diffraction techniques. SEM, coupled with EDS, was used to obtain information regarding the particle morphology and elemental distribution within the BPP sludge solids. Several SEM images of the washed solids are given in Figure S2. These images indicate highly variable particle morphologies. Spheroids with a primary size of <1 μm appeared to form aggregates that are 1−3 μm (e.g., see the upper left image in Figure S2). Needle-like structures were visible in lengths up to 40 μm (see the bottom right image in Figure S2). Rod-like structures, possibly tetragonal, were also evident (see the bottom left image in Figure S2).

Figure 2 shows a typical elemental mapping for the washed BPP sludge solids taken during the SEM examination. These images show the close association of Fe and P in the BPP sludge solids; the patterns displayed for these two elements are nearly identical. This, coupled with the FTIR result (*vide supra*) and the rapid reaction of the BPP sludge with sodium hydroxide to form ferric hydroxide (*vide infra*), would be consistent with the presence of an iron phosphate phase. The other major elemental components of the BPP sludge are also seen in the region examined, with Bi, Cr, and U appearing as ubiquitous throughout, and Na and Si displaying patterns similar to that seen for P and Fe, reflecting the topology of the sample. So, although the SEM might be supportive of the conclusion that an iron phosphate phase is present, this phase might not represent discrete iron phosphate particles, but rather a mixture with the other elements present in the sludge solids. One other feature seen in Figure 2 is an apparent correlation between Al and Na, which might suggest the presence of a sodium aluminosilicate phase.

For comparison, the SEM-EDS elemental mapping was performed on the hydrous iron(III) phosphate product prepared in this work (Figure S3). Qualitatively, the EDS map for the hydrous iron(III) phosphate was similar to that seen for the BPP sludge solids, with Na, Fe, and P mapping very closely together. There is no indication of nitrate ion in the FTIR spectrum for either the actual tank waste solids or the hydrous iron(III) phosphate, so the Na present is not in the form of entrained sodium nitrate. On the other hand, it is unclear whether the Na is entrained sodium phosphate or whether it is actually incorporated into the iron phosphate solid structure.

TEM examination was performed to glean information about the chemical form of bismuth in the BPP sludge solids because the SEM and FTIR analysis provided little relevant information in this regard. Since the FTIR clearly established that bismuth was not present as bismuth phosphate, the specific form of bismuth was not of great importance for simulant development because the bismuth is not expected to be drastically affected by caustic leaching. However, information about the bismuth species present is of importance from the standpoint of physically processing the waste, e.g., its behavior during crossflow filtration operations.

Figure S4 shows the TEM image of Bi- and Fe-rich particles in the actual tank waste. These particles (amorphous to X-rays in the bulk sample) are nearly spherical with particle diameters of about 50 nm. For comparison, Figure S4 also shows the TEM image of $BiFeO_3$, which was prepared as part of this work. The synthetic $BiFeO_3$ particles closely resemble the Bi/Fe-rich particles in the tank waste, except that the particle diameter is somewhat smaller (~20 nm). The electron diffraction pattern shows the $BiFeO_3$ particles to be amor-

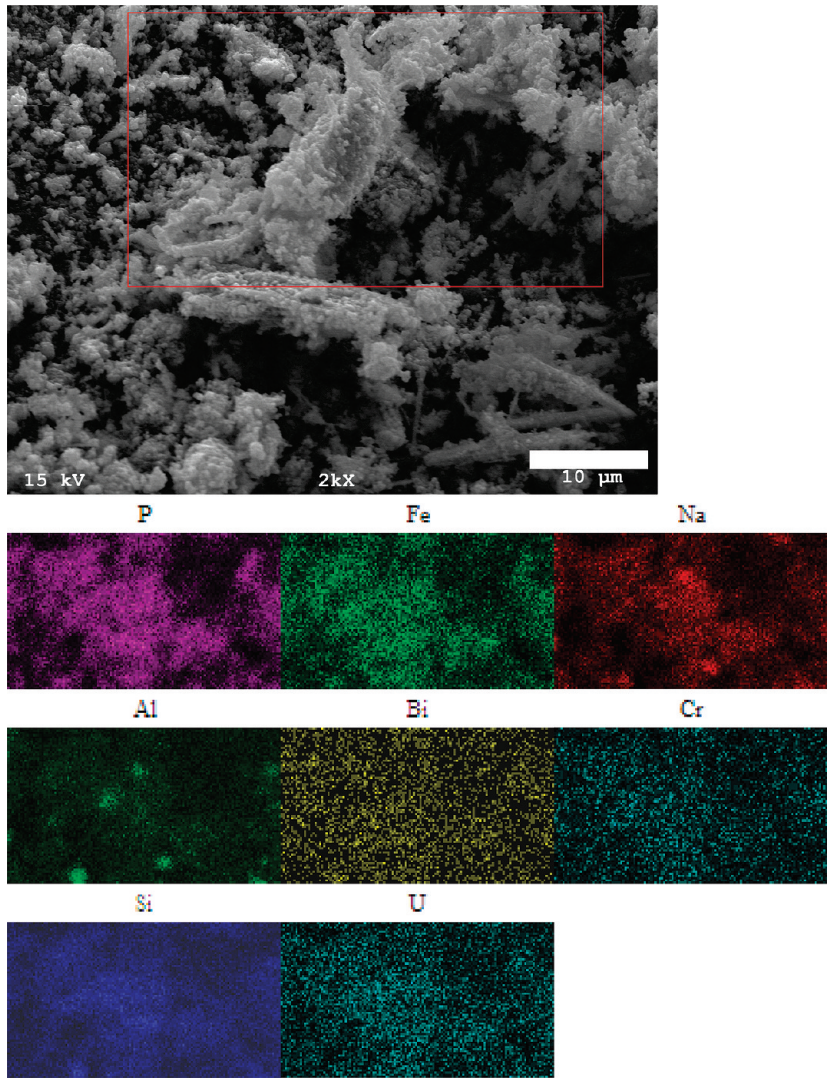

FIGURE 2. SEM image and selected EDS elemental mapping of the washed BPP sludge solids; accelerating voltage = 15 kV, K_a lines used for elemental mapping. The elemental map was taken for the upper boxed area.

phous, but these become crystalline when heated to 700 °C. Further discussion of the thermal behavior of these phases is given in the next section.

Thermal Analysis. Four TGA/DTA scans were acquired for the actual BPP sludge solids; a representative scan is shown in Figure 3. In each case, the samples lost between 20 and 24% of their initial mass. The majority of the mass loss occurred near 100 °C and was consistent with loss of waters of hydration or easily dehydrated hydroxide. Slow mass loss continued to about 500 °C. This behavior generally implies a slow bleed of hydroxide or carbonate from stable mineralized forms. Some of the bismuth oxy-hydroxides lose hydroxide as water at temperatures as high as 600 °C (*15*). The bismuth content in the solids was high enough (Table 1) that the endotherms for melting bismuth phosphate (350 °C) or bismuth oxide (824 °C) would have been evident in the DTA scans if present as pure species. But such features were not observed in the DTA scans of the BPP sludge solids.

Because the FTIR and SEM observations suggested the presence of phosphorus in the BPP sludge solids as an iron phosphate phase, TGA/DTA scans were performed on the commercially procured $FePO_4 \cdot xH_2O$ and on the hydrous iron(III) phosphate prepared in this work. Iron phosphates are reported to make glasses when heated and can encapsulate high loadings of oxides, halides, etc. (*16*). Figure S5 shows the TGA/DTA scan of commercially procured hydrated iron phosphate. The $FePO_4 \cdot xH_2O$ dehydration pattern was

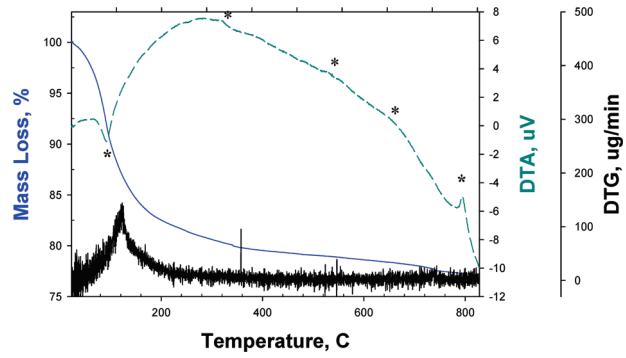

FIGURE 3. Thermal gravimetric analysis and differential thermal analysis of the water-insoluble BPP sludge solids. The scan was run at 5 °C/min to 900 °C in dry air. The large endotherm near 95 °C is loss of waters of hydration. The exothermic peaks also observed in samples bearing ferrite are shown here near 306, 544, and 730 °C and those from the hydrous iron phosphate (broad) are near 660 °C. At 794 °C exothermic change to a glassy form occurs.

quite different from that seen in the tank-waste samples. The minimum in the dehydration endotherm occurred near 185 °C in $FePO_4 \cdot xH_2O$, whereas for the tank waste solids, the minimum was near 100 °C. Bismuth oxy-hydroxide and ferric hydroxide also displayed dehydration signatures significantly

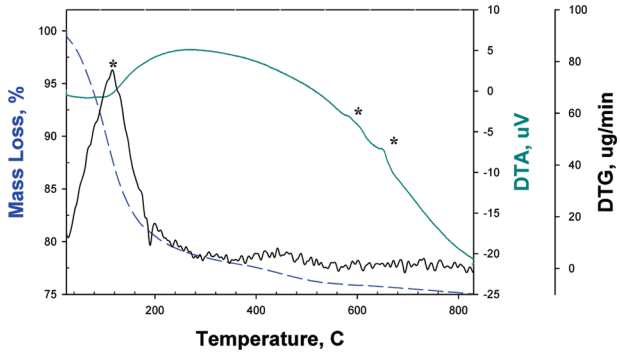

FIGURE 4. Thermal gravimetric analysis and differential thermal analysis of hydrous iron(III) phosphate. The scan was run at 5 °C/min to 900 °C in dry air. Large endotherm near 116 °C is loss of water from the hydrated salt. The exothermic peaks near 590 and 670 °C are likely due to phase transitions. Near 794 °C an exothermic change to a glass occurs.

different from that of the BPP sludge solids. For $BiO_x(OH)_y$, water loss continued to temperatures in excess of 600 °C and dehydration occurred at 65 °C for hydrous $Fe(OH)_3$. Consequently, based on known chemistries and thermal analyses, Bi_2O_3, $BiO_x(OH)_y$, $FePO_4 \cdot xH_2O$, Fe_2O_3, and $Fe(OH)_3$ can be excluded as materials that were present in significant quantities in the BPP sludge solids.

Figure 4 shows the TGA/DTA scan of the hydrous iron(III) phosphate. This material had a mass loss pattern similar to the actual tank waste sample. Exothermic transitions that occurred near 660 °C in the hydrous iron(III) phosphate sample and at 630 °C for pure iron phosphate in Figure S5 are likely similar in nature. The hydrous iron(III) phosphate material yielded a reddish glass or slag when removed from the TGA/DTA instruments. In general, the iron phosphates reported in the literature do not vitrify at temperatures below 1000 °C (*17*) and as such can be excluded, in their pure forms, as candidates for tank waste simulants since the actual waste was vitrified at much lower temperatures. For the four tank-waste samples, the observed transition temperatures that were signatures of glass or slag formation were consistently between 710 and 794 °C. The product of heating hydrous iron(III) phosphate above 660 °C was a dark brown−red cylinder that shattered like a glass. The products arising from the tank-waste samples were more robust, requiring a hammer to chip them. Thermolysis of simulant materials discussed further below indicated that the hardness of the high-temperature tank-waste products resulted partially from the presence of bismuth.

Precursors to iron phosphate glasses include materials such as hydrous sodium iron hydroxy phosphate (*16*). The main structural feature of such materials is a chain of iron ions linked by oxygen and phosphate bridges (*18*). Materials similar in structure to the hydrous sodium iron phosphate discussed above have been characterized as $3Na/Fe/2PO_4$. On a mole percent basis, Table 1 predicts similar ratios for these elements in the actual tank waste: $Na/Fe = 3$, $Na/PO_4 = 1.5-2$, $Fe/PO_4 = \sim 0.5$, $PO_4/Bi = 5-6$, $Fe/Bi = 3$, and $Na/Bi = 10$. Using these ratios, stoichiometric and excess mixtures of Bi_2O_3, $FePO_4$, Na_3PO_4, and $BiFeO_3$ were prepared and heated to 900 °C. Our simulant preparations excluded the use of SiO_2-bearing candidates such as bismutoferrite ($Fe_2^{(III)}Bi^{(III)}[OH(SiO_4)_2]$) because of the difficulty involved in synthesizing such minerals with discrete well-defined stoichiometries. It is reasonable that the combined sodium and silica content in the actual waste would induce the formation of a high-temperature (>600 °C) amorphous product. Indeed, analysis of SEM-EDS of the tank waste product suggests that this was the case.

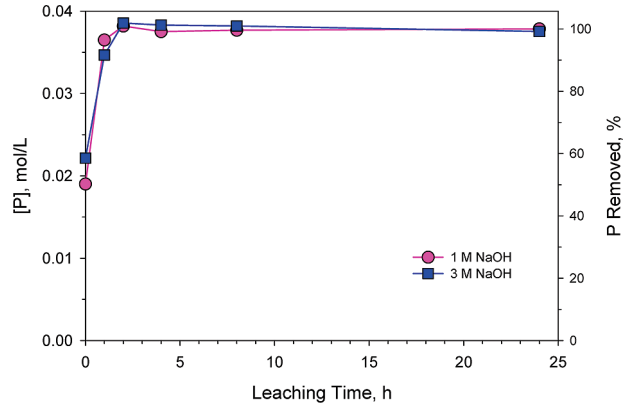

FIGURE 5. Phosphorus concentration and percent removed versus time at 60 °C for leaching of the washed BPP sludge solids in 1 and 3 M NaOH.

Mixtures high in Na_3PO_4 always produced clear soft, crushable glasses upon heating to 900 °C. Mixtures of iron as Fe_2O_3 or $Fe(OH)_3$, and bismuth as Bi_2O_3 and $Bi(OH)_3$, produced powders. Adding excess and high excesses of iron did not produce the expected reddish color observed in the actual tank waste but did make tough metallic gray amorphous material. Mixtures of $BiPO_4$ and Fe_2O_3 did not form a slag or glass at temperatures to 900 °C but remained as powders. $BiFeO_3$ by itself produced gray metallic slags that became harder above 800 °C as was observed in the actual tank waste product. However, $BiFeO_3$ contains no sodium or phosphate. Consequently, a simulant that (1) favorably reproduced the mass loss behavior in the TGA scans, (2) was compositionally representative, and (3) also produced a high-temperature product similar to those prepared from the homogenized tank waste sample was realized by thermolyzing mixtures of hydrous iron(III) phosphate and $BiFeO_3$ (see Figure S6).

Phosphorus Behavior During Caustic Leaching. The P dissolution behavior for the washed BPP sludge solids was evaluated as a function of time, temperature, and free-hydroxide concentration. Figure 5 shows the P behavior during leaching of the washed BPP sludge solids in 1 and 3 M NaOH at 60 °C. In 1 M NaOH, there was rapid transfer of P to the liquid phase. Even before heating (i.e., at $t = 0$), 50−60% of the P was removed from the solid phase. This was accompanied by the visual observation of a dramatic color change from the initial beige color of the solids to rusty-red after adding NaOH (this was seen for all conditions examined). This result points to a rapid metathesis of an iron(III) phosphate phase to sodium phosphate and ferric hydroxide. Within the experimental uncertainty, the P behavior in 1 M NaOH was essentially the same as that in 3 M NaOH at 60 °C. Similar results were obtained at 40 and 80 °C. Temperature had little influence on the P leaching kinetics. Rapid P removal was observed in all cases, typically with essentially complete removal being achieved after 2 h, and the final P concentrations were essentially the same for all test runs conducted.

The behavior of the BPP sludge solids during treatment with NaOH is well mimicked by that of hydrous iron(III) phosphate. Adding aqueous NaOH to the hydrous iron(III) phosphate results in a rapid change in color from beige to rusty-red, indicating conversion to ferric hydroxide and sodium phosphate. The commercially procured $FePO_4 \cdot xH_2O$ also behaves in this manner. But because of its crystalline nature, its pink (rather than beige) color, and its somewhat different FTIR spectrum (Figure 1), the commercially manufactured $FePO_4 \cdot xH_2O$ is not believed to be the best candidate to simulate the actual waste. Rather, the hydrous material formed by mixing ferric nitrate with sodium phosphate is

believed to more closely mimic the phosphorus present in the tank waste.

Acknowledgments

Pacific Northwest National Laboratory is operated for the U.S. Department of Energy by Battelle under Contract DE-AC05-76RL01830. This work was funded by the U.S. Department of Energy through the Office of Environmental Management and under the guidance of Bechtel National, Inc.

Supporting Information Available

Schematic of the main operations to be performed in the Hanford WTP along with figures containing an elemental EDS map and TGA/DTA scans. This material is available free of charge via the Internet at http://pubs.acs.org.

Literature Cited

(1) Hileman, B. Energy Department has Made Progress Cleaning Up Nuclear Weapons Plants. *Chem. Eng. News* **1996**, *74* (30), 14–20.

(2) Stewart, T. L.; Frey, J. A.; Geiser, D. W.; Manke, K. L. Overview of U.S. Radioactive Tank Problem. In *Science and Technology for Disposal of Radioactive Tank Wastes*; Schulz W. W., Lombardo, N. J., Eds.; Plenum Press: New York, 1998; pp 3−13.

(3) Lumetta, G. J.; Rapko, B. M.; Liu, J.; Temer, D. J. Enhanced Sludge Washing for Pretreating Hanford Tank Sludges. In *Science and Technology for Disposal of Radioactive Tank Wastes*; Schulz W. W., Lombardo, N. J., Eds.; Plenum Press: New York, 1998; pp 203−218.

(4) Lumetta, G. J.; Rapko, B. M. Removal of Chromium from Hanford Tank Sludges. *Sep. Sci. Technol.* **1999**, *34*, 1495–1506.

(5) Sylvester, P.; Rutherford, L. A., Jr.; Gonzalez-Martin, A.; Kim, J.; Rapko, B. M.; Lumetta, G. J. Ferrate Treatment for Removing Chromium from High-Level Radioactive Tank Waste. *Environ. Sci. Technol.* **2001**, *35*, 216–221.

(6) Fiskum, S. K.; Arm, S. T.; Steele, M. J.; Thornson, M. R. Spherical Resorcinol-Formaldehyde Performance Testing with Hanford Tank Waste. *Solvent Extr. Ion Exch.* **2008**, *26*, 435–452.

(7) Lumetta, G. J.; Rapko, B. M.; Cho, H. M. Studies of the Fundamental Chemistry of Hanford Tank Sludges. In *Proceedings of the 9th International Conference on Environmental Remediation and Radioactive Waste Management*; The American Society of Mechanical Engineers: Fairfield, NJ, 2003; Session 9, Paper 5.

(8) Cleveland, J. M. *The Chemistry of Plutonium*; Gordon and Breach Science Publishers: New York, 1970; pp 500−503.

(9) Bartonickova, E.; Cihlar, J.; Castkova, K. Microwave-assisted synthesis of bismuth oxide. *Proc. Appl. Ceram.* **2007**, *1*, 29–33.

(10) Shwetha, S.; Palkar, V. R.; Pinto, R. Size effect study in magnetoelectric $BiFeO_3$ system. *PRAMANA-J. Physics* **2002**, *58*, 1027–1030.

(11) Lumetta, G. J.; Buck, E. C.; Daniel, R. C.; Draper, K.; Edwards, M. K.; Fiskum, S. K.; Hallen, R. T.; Jagoda, L. K.; Jenson, E. D.; Kozelisky, A. E.; MacFarlan, P. J.; Peterson, R. A.; Shimskey, R. W.; Sinkov, S. I.; Snow, L. A. *Characterization, Leaching, and Filtration Testing for Bismuth Phosphate Sludge (Group 1) and Bismuth Phosphate Saltcake (Group 2) Actual Waste Sample Composites*; PNNL-17992 (WTP-RPT-166); Pacific Northwest National Laboratory: Richland, WA, 2009.

(12) de Barry Barnett, E.; Wilson, C. L. *Inorganic Chemistry: A Text-Book for Advanced Students*; Longmans Green and Co: London, 1953; p 202.

(13) Żegliński, J.; Piotrowski, G. P.; Piekoś, R. A study of interaction between hydrogen peroxide and silica gel by FTIR spectroscopy and quantum chemistry. *J. Mol. Struct.* **2006**, *794*, 83–91.

(14) Liu, Q.; Xu, H.; Navrotsky, A. Nitrate cancrinite: Synthesis, characterization, and determination of the enthalpy of formation. *Micro. Meso. Mater.* **2005**, *87*, 146–152.

(15) Christensen, A. N.; Jensen, T. R.; Scarlett, N. V. Y.; Madsen, I. C.; Hanson, J. C.; Altomare, A. In-situ X-ray powder diffraction studies of hydrothermal and thermal decomposition reactions of basic bismuth(III) nitrates in the temperature range 20−650°C. *Dalton Trans.* **2003**, 3278–3282.

(16) Kim D. S.; Buchmiller, W. C.; Schweiger, M. J.; Vienna, J. D.; Day, D. E.; Kim, C. W.; Zhu, D.; Day, T.; Neidt, T.; Peeler, D. K.; Edwards, T. B.; Reamer, I. A.; Workman, R. J. *Iron Phosphate Glass as an Alternative Waste-Form for Hanford LAW*; PNNL-14251; Pacific Northwest National Laboratory: Richland, WA, 2003.

(17) Scaccia, S.; Carewska, M.; Di Bartolomeo, A.; Prosini, P. P. Thermoanalytical investigation of iron phosphate obtained by spontaneous precipitation from aqueous solutions. *Thermochim. Acta* **2002**, *383*, 145–152.

(18) Bridson, J. N.; Quinlan, S. E.; Peter, R. Synthesis and Crystal Structure of Maricite and Sodium Iron(III) Hydroxyphosphate. *Chem. Mater.* **1998**, *10*, 763–768.

ES9013745